Synthesis of Cu doped NiO for Their Antioxidant and Photocatalytic Properties: Green Synthesis Using Lycopodium Linn

S. R. Bavaji

bavajibavaji774@gmail.com

Jamal Mohamed College (Autonomous), Affiliated to Bharathidasan University

A. Jafar Ahamed

Jamal Mohamed College (Autonomous), Affiliated to Bharathidasan University

P. Rajeswaran

Vel Tech High Tech Dr.Rangarajan Dr.Sakunthala Engineering College (Autonomous)

Research Article

Keywords: ZnO@ZnS, Hydrothermal, UV light, MO dye, Photocatalyst

Posted Date: December 14th, 2023

DOI: https://doi.org/10.21203/rs.3.rs-3726422/v1

Additional Declarations: No competing interests reported.

Version of Record: A version of this preprint was published at Chemical Physics Impact on May 1st, 2024. See the published version at https://doi.org/10.1016/j.chphi.2024.100647.

Abstract

When compared to metal oxide nanoparticles made via physical and chemical processes, those made using botanical extracts are more stable and biocompatible. Evaluation of the antioxidant and photocatalytic properties of NiO NPs synthesized from Phytolacca dodecandra L. Herit (P.d) leaf extract is the primary objective of this study. The produced Cu-doped NiO-NPs at an optimal temperature of 400 ^{o}C have been studied using XRD, TEM, FT-IR, UV-Vis, BET, and XPS studies at varying concentrations of copper (1, 3, and 5%). Dye water solutions of Rose Bengal (RB) and Methylene Blue (MB) were degraded to test the photocatalytic activity of the produced samples. When exposed to UV light for 60 minutes, 5-Cu-NiO nanophotocatalyst degraded MB dye at a rate of 98.7% (0.5 mol/L), with a high apparent constant of 0.9871 min^{-1} and excellent long-term stability. At concentrations of 363.96 and 350.29 g/mL, respectively, NiO NPs and CuNiO NPs inhibited the oxidation of 50% of the H_2O_2 molecules in the antioxidant test. In addition, copper ions may be responsible for the increased antioxidant activity of the biosynthesized NiO NPs.

1. Introduction

Numerous natural and anthropogenic impacts have been felt on the Earth's crust, leading to a number of new environmental issues. Deterioration of the natural world as a result of human activity is generally understood to include pollution in the broadest sense [1]. Changes to the biological, chemical, and physical characteristics of natural water sources impact not just human health but also marine ecosystems [2]. Overpopulation, urbanization, and increasing industrialisation are only a few examples of the many factors contributing to the contamination of the world's freshwater supplies [3–5]. Industries involving the manufacturing of grains, dyes, pulp, and colors are the primary contributors to water pollution. Organic dye pollution has an active role in damaging marine ecosystems [6–8]. In case you forgot, dyes are molecules of organic matter with the aromatic ring structure that absorb light in the visible spectrum to produce color. The textile, culinary, cosmetic, pharmaceutical, and other businesses that make use of this vital quality are major contributors to water pollution because they use large quantities of hazardous dyes in their production processes. Methylene blue (MB) is one of the most popular dyestuffs used in the textile industry for shading silk, wool, cotton, linen, etc. Despite its widespread usage, MB is poisonous and carcinogenic since it is found in wastewater released by the textile industry. Non-biodegradable substances pose a significant risk to human and environmental health [9]. As a result, photocatalysis has emerged as an intriguing option for the comprehensive mineralization of a wide range of dye contaminants found in sewage. In this study, MB is eliminated using photodegradation, a sophisticated oxidation method [10, 11].

When it comes to using solar energy via photovoltaic and water-splitting systems to alleviate the energy and environmental crises, wide band gap semiconductors like TiO_2, ZnO, etc. have immense promise [12, 13]. Their limited usefulness is due to the fact that their broad band-gaps prevent them from using visible light. Consequently, in order to make effective use of solar energy, it is crucial to create new types of photo catalysts with high activity in visible light. NiO NPs have the highest capacity of any metal oxide

NPs in scavenging ROS. The hydroxyl radical scavenging capability of NiO NPs produced through a simple green combustion technique employing Limonia acidissima natural fruit juice is particularly impressive [14]. With an IC50 of 258 g/mL [15], the antioxidant potential of biosynthesized NiO NPs produced using Raphanus sativus peel and calcined at 100 ^{o}C was the highest. Because of their cheap cost, energy efficiency, and lack of toxicity compared to chemical techniques, biological methods of manufacturing NPs employing microorganisms including algae, fungus, bacteria, and plant leaf extracts have been proposed as potential environmentally acceptable replacements to chemical methods [16, 17]. Plants have a wide variety of phytochemicals that might help in reduction, are non-toxic, and can be used in the synthesis of NPs. Since this is the first in-depth report on P. dodecandra L. Herit being used for green synthesis of NiO NPs and CuNiO NPs, its leaf extracts are being taken into consideration in the current investigation. This is the first time Cu doped NiO has been employed as a nanocatalyst for photodegradation of organic dyes and antioxidant activity through green synthesis, as far as we are aware. The process and mechanism of photodegradation were studied in great detail by analyzing its structure and morphology.

2. Experimental section

2.1. Materials

The leaves of P. dodecandra L. Herit were utilized with nickel nitrate hexahydrate, methylene blue, hydrogen peroxide, sodium hydroxide, phosphate buffer, sulfuric acid, nitric acid, chloroform, Wagner's solution, ferric chloride, a solution of concentrated hydrochloric acid, ascorbic acid, distilled water, and a few more chemicals. In this experiment, only high-quality analytical agents and substances were employed.

2.2. Sample Collection and Preparation.

After being randomly sampled from the Jimma University Garden in Jimma, Southwest Ethiopia, the P.dodecandra L'Herit (P.d) leaves were washed with tap water to remove dirt and other pollutants, rinsed again with distilled water, and then air-dried at room temperature. The dried sample was crushed using a pestle and then 10 grams of leaves were boiled in 100 milliliters of distilled water at about 60 degrees Celsius for 20 minutes to make an aqueous extract of the leaf. The extract was filtered using Whatman No. 1 filter paper after being cooled to room temperature. The extract was then kept for further use in research.

2.3. Synthesis of pure and Cu doped NiO nanoparticles

After stirring 50 mL of 0.1 M nickel(II) nitrate hexahydrate ($Ni(NO_3)_2.6H_2O$) for 20 minutes, 20 mL of leaf extract was added dropwise to complete the production of NiO NPs. A magnetic stirrer set to 4000 rpm was used to gradually swirl the liquid for 30 minutes at room temperature. Drop by drop, 5 M NaOH was added to the solution until the pH was corrected to 10. After 2 hours of stirring at ambient temperature, the resulting mixture was centrifuged for 10 minutes to separate the precipitate, which was then washed

several times with ethanol and distilled water to eliminate any remaining contaminants before being dried in an oven at 70 degrees Celsius for another 2 hours. The powder was then dried some more and calcined in a muffle furnace at 400 degrees for two hours. Additional research made use of the product. Drop by drop, 20 mL of leaf extract was mixed with 50 mL of 0.1 M nickel(II) nitrate hexahydrate ($Ni(NO_3)_2.6H_2O$) to create the CuNiO catalyst for the production of Cu doped NiO. The pH of the solution was adjusted to 10 by gradually adding 5 M NaOH. After 2 hours of stirring at ambient temperature, the resulting mixture was centrifuged and rinsed with ethanol and distilled water to eliminate any remaining contaminants before being dried in an oven at 70 degrees Celsius for another 2 hours. The obtained powder was calcined for two hours at 400 degrees Celsius. One-percent Cu-doped NiO (1-Cu-NiO), three-percent Cu-doped NiO (3-Cu-NiO), and five-percent Cu-doped NiO (5-Cu-NiO) were created. In Fig. 1(a) we see a simplified diagram of the synthesis process.

2.4. Photocatalytic set up

The degradation of MB dye under UVA-light (11W) irradiation was used to investigate the photocatalytic activity of Cu-doped NiO-NPs [18]. The degradation and photocatalytic process of this pigment began with the use of UV-Vis spectrophotometry. To do this, 50 mL of MB solution (10 − 5 M, pH = 9) was added to 0.03 g of Cu-doped NiO-NPs. After mixing the photocatalyst and pigment solution in the dark for 30 minutes, we subjected the mixture to UVA-light to achieve adsorption-desorption stability. After 100 minutes of stirring intermittently under UV light, the solution was tested. After that, UV-Vis spectroscopy was used to detect the adsorption at every fifteen minutes.

3. Results and discussion

3.1. XRD analysis

The structural and crystallographic data of Cu-doped NiO-NPs at various concentrations and 400 ^{o}C are shown in Fig. 1 (b). These nanoparticles have a cubic (fcc) crystal structure, as shown by the presence of five signal peaks in the range 2 (10-90^{o}): the (111), (200), (220), and (222) planes [19, 20]. The absence of any other maxima in this picture is further evidence that the generated nanoparticles are very pure. The information collected has been according to the norm (JCPDS # 04-0835). As the copper content rises, the size of the nanoparticles grows and the strength of the peaks falls. As the concentration increases, the growth rate increases, and the internal structure weakens, causing this induction. Nanoparticle sizes may be estimated using the Scherer equation [21]. It has been reported that pure NiO-NPs have a size of 26.1 nm, whereas Cu-doped NiO-NPs have been identified to have a size of 17.5–35.8 nm at concentrations of 1–5%. In Fig. 1 (c), the crystal structure of NiO was also shown for your perusal.

3.2. Morphological analysis

SEM analysis revealed the materials' topological, morphological measurement, and compositional details. SEM micrographs of pure and Cu doped NiO nanoparticles are shown in Fig. 2 (a-c), where it is evident that the nanoparticles are randomly agglomerated and vary in size from nanometers to microns.

TEM allowed for the identification of the distinct morphological data. In Fig. 2(d), virgin NiO is shown as spherical, agglomerated nanoparticles in a transmission electron micrograph. Figure 2(e) is a transmission electron micrograph of 5-Cu-NiO, which reveals the spherical nanoparticles with a diameter between 20 and 35 nm, with some bigger aggregates present. The high surface energy and strain of Cu doped NiO NPs cause them to aggregate, which may account for the discovery of certain particularly big nanoparticles. The produced nanomaterials are polycrystalline and as shown by the SAED pattern for 5-Cu-NiO shown in Fig. 2(f).

3.3. FTIR spectra analysis

As can be seen in Fig. 3(a), the FTIR spectra of NiO and Cu-NiO nanomaterials were obtained between 4000 and 400 cm^{-1}. The bending and stretching vibrations of -OH account for the wide peak at 3431 and 1643 cm^{-1}, which is caused by the absorbed water on the catalyst's surface [22, 23]. The existence of water on the NiO surface causes large absorption bands at 2871–3323 cm^{-1} owing to H–O–H or N–H stretch. The absorption band at 1376 cm^{-1} is caused by the alcohol's bending vibration. NiO powder is nanoparticles and crystallized, as seen by the bands' width. The peaks at 745–480 cm^{-1} originate from the Ni–O stretching vibration mode. Signature areas of stretching vibrations in the atoms account for the absorption bands seen between 1500 and 1400 cm^{-1}. Finally, a band can be seen in the range of 500 – 450 cm^{-1}, which corresponds to the stretching vibration of Cu-doped NiO. The data shows that as the threshold concentration of copper is exceeded, the peaks become more intense [24].

3.4. Optical studies

Optical absorption measurement (UV-Vis spectroscopy) was used to study the morphological and spectral features of pure and Cu doped NiO photocatalysts. The UV-Vis spectra of both unadulterated and Cu-doped NiO photocatalysts are shown in Fig. 3(b). The resultant figure shows an increase in the UV-Vis spectra due to Cu-doped metal, which may be attributed to a change in surface shape. As a result of its asperity, the doped metal increases the dispersion of light since it is composed of bigger particles. XRD analysis further corroborated the growing size of the crystals. Tauc's equation was used to calculate the bandgap of photocatalysts. As shown in Fig. 3 (c), the bandgap value may be calculated by extrapolating the linear portion of a graph of $(\alpha h\nu)^2$ against eV.. Bandgap values of 3.17 eV, 3.11 eV, 2.88 eV, and 2.65 eV have been calculated for NiO, 1-Cu-NiO, 3-Cu-NiO, and 5-cu-NiO photocatalysts, respectively. Bandgap narrowing of the Cu-NiO photocatalyst was reported in the presence of Cu-doped metal. Bandgap values have been shown to decrease in this way (with larger crystallites) in prior research [25, 26]. Replacement of ions (Cu^{2+} and Ni^{2+}) in the framework of the host semiconductor (NiO) may produce a decrease in the band gap value of Co-doped metal. Pure and Cu-doped NiO both exhibit two distinct emission peaks at 380 and 534 nm on the photoluminescence spectrum (Fig. 3d). Band edge emission are responsible for the prominent peak at 534 nm. Peak values are lower in Cu doped NiO compared to undoped NiO because radiation recombination is suppressed. The photoluminescence signals are weaker when recombination rates are lower, which may be advantageous when trying to improve photocatalytic performance.

3.5. Surface area and elemental composition analysis

Surface area was determined by subjecting pure and Cu-doped NiO nanoparticles to a BET nitrogen absorption test (Fig. 4a). Adsorption isotherm measurements of particle surface area corroborate the presence of a type IV isotherm, suggesting that the particles may have a mesoporous structure [27–30]. Surface areas of 45.5 m2/g for NiO and 94.1 m2/g for 5-Cu-NiO have been computed. According to the BJH technique, the pore volume distribution for NiO and 5-Cu-NiO are 0.3225 cm3 /g and 0.0181 cm3 /g, respectively, with an average, uniform pore size distribution of 23.7 nm and 33.5 nm. The effect of Cu doping on the valence state of NiO has been verified by analyzing XPS spectra of Cu-doped NiO. The complete XPS spectra of 5-Cu-doped NiO samples are shown in Fig. 4c, and they are indicative of the existence of Ni, Cu, and O. Detailed analysis and presentation of the XPS high-resolution spectra are shown in Fig. 4d. The 2p3/2 and 2p1/2 peaks account for the Ni 2p signals at 853.1 eV and 875.3 eV, correspondingly [31]. The corresponding XPS spectra of the Cu 2p component level in the doped sample is shown in Fig. 4e. Cu2p signals, which correspond to 2p3/2 and 2p1/2 in the periodic table, can be seen at 932.9 and 953.2 eV in the recorded spectra. Peaks at 531.2 and 529.3 eV in the O1s spectra shown in Fig. 4d may correspond to oxygen ion departures from Cu-doped NiO [32].

3.6. Photocatalytic studies

As a test response, we used photocatalytic decomposition of MB and RB dyes to gauge the produced sample's potential for degrading organic contaminants. It was decided to use the photocatalytic degradation procedure while measuring the typical absorbance of MB at 664 nm and RB at 525 nm. Absorption spectra of MB and RB dyes with and without all photocatalyst samples and sunshine are given in Fig. 5 (a-d), respectively. The spectra of absorption show that it fades away with time. Dye degradation caused by exposure to sunshine and artificially produced samples is reflected in a decrease of absorption band intensities. A chromophore with a lengthy chained system may be responsible for the 664 nm absorption band typical of MB. The reduction of the absorbance band at 664 nm [33] indicated that the conjugated link in the MB molecule structure had been disrupted. The curve of the degradation efficiency vs absorption value is shown in Fig. 6 (a & b). The photocatalytic degradation rate of MB in 60 minutes was 41% in the presence of bare NiO and 99% in the presence of 5-Cu-NiO photocatalyst. This is likely due to the fact that the Cu dopant increases the photocatalyst's active site count. After 60 minutes, the photocatalyst effect of 5% Cu doped-NiO-NPs on RB dye degradation was around 78%. There are likely more free electrons and holes available for the production of free radical that is ions because copper ions have been included into the NiO-NPs lattice, which decreases the recombination of electron-hole pair owing to the broad energy band [34]. The data indicated that the process followed a pseudo-first-order kinetics. The linear relationship between Ln(Ct C_0) and light duration is seen in Fig. 6 (c & d). For the 5-Cu-NiO photo catalyst, the maximum rate constant toward MB dye was around k = 0.7681 min^{-1}. Table.1 also showed the rate constant for each photocatalyst sample. A photocatalyst's reusability is crucial for determining its efficacy. The catalyst was recovered from the reaction media once deterioration was complete and put through a reusability test. The catalyst was recovered by centrifuging the deteriorated solution at 3000 rpm while discarding the supernatant. For photocatalysis,

the photocatalyst was subjected to sunlight for 60 minutes. Using a UVvis spectrophotometer, the quantities of degraded dyes were determined in 5 mL of the dye solutions extracted at the specified times. Figure 7 (a & b) demonstrates the efficacy of NiO NP and 5-Cu-NiO photocatalysts in removing MB and RB. The data indicated that even after 5 iterations, the removal performance dropped by just 2%to 4%. Since CuNiO nanocomposites show strong stability and reusability performance, they are a promising choice for real-world photocatalysis applications [35], and repeated applications for the photocatalytic process show a modest reduction in MB degradation. Finally, different catalysts [36–40] used to get rid of organic pollutants were compared to the results obtained with the present catalyst in terms of photocatalytic activity (Table 2). The present photocatalyst, Cu-doped NiO-NPs, has been shown to achieve a better degradation % in a short amount of time. At an optimum pH and an irradiation period of 60 min, the impact of the level of dye on the degrading ability of the catalyst was examined by varying the starting dye concentration from 5 to 10 to 15 mg/L. After 30 minutes of being held in the dark, the adsorptiondesorption equilibrium between the NPs in MB and RB liquid was reached. The efficiency with which the catalyst degrades the dye is inversely proportional to the starting concentration of the dye, as seen in Fig. 7 (c & d). Time required for full degradation and photocatalytic efficiency both decrease with increasing starting dye concentration of MB. When there is a lot of a dye in the system, a lot of its molecules will be adsorbed on the catalyst surface, making it darker. Dye degradation was investigated as a function of photocatalyst mass, with all other experimental factors held constant. At an ongoing dye level of 10 mg/L, the percentage of MB degradation was evaluated for a range of catalyst levels from 20 to 60 mg, which is consistent with and lower in dosage than a previous research [41]. As additional active sites on the surface of the catalyst become available, the photocatalytic activity continues to rise in response to an increase in the reactive load.

Table 1
Photocatalytic activity parameters of pure and Cu doped NiO photocatalyst samples

Samples	Rate constant of MB		Rate constant of RhB		MB Degradation efficiency (%)	RB Degradation efficiency (%)
	K (h^{-1}) min^{-1}	R^2	K (h^{-1}) min^{-1}	R^2		
NiO	0.0913	0.997	0.0276	0.999	41	27
1-Cu-NiO	0.2121	0.987	0.1121	0.985	56	41
3-Cu-NiO	0.4541	0.985	0.2239	0.981	72	56
5-Cu-NiO	0.7681	0.999	0.3498	0987	99	78

Table 2
A comparison of photodegradation of MB between present work and already reported Cu-NiO based materials.

Catalyst	Light source	Dye	Time (min)	Degradation (%)	Ref.
Cu doped NiO NPs	Visible	EBT and MB	90	51	[36]
Cu doped NiO NPs	Sun light	MB	60	89	[37]
Cu doped NiO NPs	Visible	Alizarin red	60	90	[38]
Mn doped NiO NPs	UV light	MB	210	92	[39]
Co doped NiO NPs	Visible	MB	50	89	[40]
Cu doped NiO NPs	UV light	MB	60	99	This work

3.7. Antioxidants analysis

Having the capacity to contribute hydrogen or electrons to the oxidants is the primary feature of anti-oxidants, which are defined by their ability to scavenge free radicals. The levels of 1,000, 750, 500, 250, 100, and 50 g/mL were used to calculate the predicted scavenging activities of the particles. Figure 8c displays the computed IC50 values of 349.8 and 362.87 g/mL for 5-Cu-NiO NCs and NiO NPs, respectively, demonstrating the efficient free radical scavenging activity of the synthesized materials in comparison to ascorbic acid (301.56 g/mL). The IC50 figures show that radicals may be suppressed. The presence of polyphenols may account for the outcome. In plants, phenols are the most widespread secondary metabolites. They are recommended for use in the treatment of many illnesses due to their high antioxidant content and other beneficial biological features [42]. The photocatalytic degradation mechanism of MB on Cu doped NiO is shown schematically in Fig. 9. UV light with an energy equal to or greater than the band gap of energy of NiO excited an electron in the valence band (VB) to the conduction band, simultaneously generating a hole (h^+) in the VB, and the Mn nanoparticles on the NiO surface acted as a sink for electron to improve the electron-hole pair separation. By combining with oxygen (O_2), the excited electron creates the superoxide radical anion ($\bullet O_2^-$). While positive holes may oxidize contaminants directly, they most often react with surface-bound water (OH^-) to form the hydroxyl radical (•OH), which serves as the center of activity in photocatalytic processes. The oxidation of MB dye by •OH or $\bullet O_2^-$ radicals is the mechanism by which it degrades. In photocatalytic oxidation reactions, these radicals are the reactive oxygen species (ROS). These radicals are easier to produce because to the increased charge separation rate, which aids in the bleaching of MB. In addition, the incorporation of NiO with Cu^{2+}, which may mediate interfacial transfer of charge, may be responsible for the material's increased photocatalytic activity (NiO:Mn).

4. Conclusions

By employing P. dodecandra L. Herit's leaf extract as a capping and reduction agent, a simple, clean, economically feasible, and environmentally friendly method for synthesizing NiO NPs and CuNiO NCs

has been created. The XRD pattern revealed that increasing the copper content led to bigger nanoparticles. In the instance of a 1% concentration, the FESEM pictures showed cubes, whereas those taken at a 3% and 5% concentration showed spheres. When exposed to UV light for 60 minutes, 5-Cu-NiO nanophotocatalyst degraded MB dye at a rate of 98.7% (0.5 mol/L), with a high apparent constant of 0.9871 min^{-1} and excellent long-term stability. At concentrations of 363.96 and 350.29 g/mL, respectively, NiO NPs and CuNiO NPs inhibited the oxidation of 50% of the H_2O_2 molecules in the antioxidant test. The results of the photocatalytic tests show that the synthetic samples have great potential as photocatalysts for the elimination of organic contaminants. This research emphasizes the accomplishments in the area of photocatalysis and provides a green and nontoxic technique to synthesis nanomaterials utilizing an ecofriendly preparation approach, which is useful for the future work in applications in industry.

Declarations

Acknowledgement

Not applicable

Conflicts of interest

The authors declare that there is no conflict of interest regarding the research work reported in this manuscript.

Author contributions

S.R. Bavaji and A. Jafar Ahamed, , study conceptualization and writing (original draft) the manuscript **P. Rajeswaran,** data curation, formal analysis and writing (review & editing).

Data and code availability statement

The data that support the findings of this study are available from the corresponding author, upon reasonable request.

Supplementary information

Not applicable

Financial interest

The authors have no relevant financial or non-financial interests to disclose.

Ethical approval

The authors declare that there is no human cells and tissues are used in this manuscript.

References

1. S. Horoz, O. Baytar, O. Sahin, H. Kilicvuran, Photocatalytic degradation of methylene blue with Co alloyed CdZnS nanoparticles. J. Mater. Sci. Mater. Electron. 29 (2018) 1004–1010.
2. K. Jyotsna, A. Tandon, A nonlinear mathematical model investigating the sustainability of an urban system in the presence of haphazard urban development and excessive pollution. Nat. Resour. Model. 31 (2018) e12163.
3. N.M.P. Rana, Urbanization and sustainability: challenges and strategies for sustainable urban development in Bangladesh. Environ. Dev. Sustain. 13 (2011) 237–256.
4. Benjamin Ayim-Otu, Melih Kuncan, Ömer Şahin, Sabit Horoz, Synthesis and photovoltaic application of ZnS:Cu (3%) nanoparticles. J. Aust. Ceram. Soc. 56 (2020) 639-643.
5. Nattikran Yuangpho, Dang T. T. Trinh, Duangdao Channei, Wilawan Khanitchaidecha & Auppatham Nakaruk, The influence of experimental conditions on photocatalytic degradation of methylene blue using titanium dioxide particle. J. Aust. Ceram. Soc. 54 (2018) 557–564.
6. M. Coto, S.C. Troughton, J. Duan, R.V. Kumar, T.W. Clyne, Development and assessment of photo-catalytic membranes for water purification using solar radiation. Appl. Surf. Sci. 433 (2018) 101–107.
7. Orhan Baytar, Omer Sahin, Hilal Kilicvuran, Sabit Horoz, Synthesis, structural, optical and photocatalytic properties of Fe-alloyed CdZnS nanoparticles. J. Mater. Sci. Mater. Electron. 29 (2018) 4564–4568.
8. Chunliang Hang, Lixia Yang, Rencheng Jin, Feng Wang, Guihua Li & Yanbin Xu, Porous CeB 6 nanostructure: a step towards rapid adsorption of methylene blue. J. Aust. Ceram. Soc. 54 (2018) 423–428.
9. Shakeel Ahmed, Mudasir Ahmad, Babu Lal Swami, Saiqa Ikram, A review on plants extract mediated synthesis of silver nanoparticles for antimicrobial applications: a green expertise. J. Adv. Res. 7 (2016) 17–28.
10. S.A. El-Hakam, F.T. ALShorifi, R.S. Salama, S. Gamal, W.A. El-Yazeed, A.A. Ibrahim, A.I. Ahmed, Application of nanostructured mesoporous silica/ bismuth vanadate composite catalysts for the degradation of methylene blue and brilliant green. J. Mat. Res. Technol. 18 (2022) 1963–1976.
11. L. Sun, D. Hu, Z. Zhang, X. Deng, Oxidative degradation of methylene blue via PDS-based advanced oxidation process usingnatural pyrite. Int. J. Environ. Res. Public Health 16 (2019) 4773.
12. Y. Li, X. Fang, N. Koshizaki, T. Sasaki, L. Li, S. Gao, Y. Shimizu, Y. Bando, and D. Golberg, “Periodic TiO2 Nanorod Arrays with Hexagonal Nonclose-Packed Arrangements: Excellent Field Emitters by Parameter Optimization”, Advanced Functional Materials, Vol. 19, No.15, pp. 2467-73, Aug 2009.
13. Y. Qiu, K. Yan, H. Deng, and S. Yang, “Secondary branching and nitrogen doping of ZnO nanotetrapods: building a highly active network for photoelectrochemical water splitting”, Nano letters, Vol. 12, No. 1, pp. 407-13, Dec 2011

14. M.S.S. Kumar, T.L. Soundarya, G. Nagaraju, G.K. Raghu, N.D. Rekha, F.A. Alharthi, B. Nirmala, Multifunctional Applications of Nickel Oxide (NiO) Nanoparticles Synthesized by Facile Green Combustion Method Using Limonia Acidissima Natural Fruit Juice. Inorg. Chim. Acta. 515 (2020) 120059.
15. MA.M. Rashid, M. Rahman, A.O. Mahmud, A.S. Morshed, M. Haque, M.M. Hossain, UV-Vis Spectrophotometer as an Alternative Technique for the Determination of Hydroquinone in Vinyl Acetate Monomer. Photochem. 2 (2022) 435–447.
16. Z. Getu, Green Synthesis and Nanoparticles Using Endod (Phytolacca dodecandra) Leaf Extract and Evaluation Of antimicrobial activities. J. King Saud Univ. – Sci. 32 (2019) 2358–2364.
17. F. Sabir, E. Bekele, B. Gonfa, G. Edossa, A. Adino, Synthesis of Cobalt Oxide Nanoparticles Through Chemical and Biological Pathways for Antibacterial Activity. J. Nanostructures. 11 (2021) 577–587.
18. S.H. Amirnordin, H.A. Rahman, H.Z. Abdullah, H. Taib, Effect of Zeta Potential of Stanum Oxide (SnO_2) on Electrophoretic Deposition (EPD) on Porous Alumina, Advanced Materials Research, Trans Tech Publ, 2013, pp. 334–337.
19. S.A. Khan, S. Shahid, A. Ayaz, J. Alkahtani, M.S. Elshikh, T. Riaz, Phytomolecules-coated nio nanoparticles synthesis using abutilon indicum leaf extract: antioxidant, antibacterial, and anticancer activities, Int. J. Nanomed. 16 (2021) 1757.
20. G. Tong, Q. Hu, W. Wu, W. Li, H. Qian, Y. Liang, Submicrometer-sized NiO octahedra: facile one-pot solid synthesis, formation mechanism, and chemical conversion into Ni octahedra with excellent microwave-absorbing properties, J. Mater. Chem. 22 (2012) 17494–17504.
21. M. Parthibavarman, M. Karthik, P. Sathishkumar, R. Poonguzhali, Rapid synthesis of novel Cr-doped WO_3 nanorods: an efficient electrochemical and photocatalytic performance, J. Iran. Chem. Soc. 15 (2018) 1419-1430.
22. P. L. Hower, T.K. Gupta, A barrier model for ZnO varistors, Journal of Applied Physics, 50 (1979) 4847-4855.
23. R. Wahab, S. G. Ansari, Y. S. Kim, H. K. Seo, G. S. Kim, G. Khang, and H. S. Shin, Low temperature solution synthesis and characterization of ZnO nano-flowers, Materials Research Bulletin. 42 (2007) 1640-1648.
24. K. Sathishkumar, N. Shanmugam, N. Kannadasan, S. Cholan, G. Viruthagiri, Influence of Zn^{2+} ions incorporation on the magnetic and pseudo capacitance behaviors of NiO nanoparticles, Mater. Sci. Semicond. Process. 27 (2014) 846–853.
25. R. He, R.K. Hocking, T. Tsuzuki, Local structure and photocatalytic property of mechanochemical synthesized ZnO doped with transition metal oxides. J. Aust. Ceram. Soc. 49 (2013) 70–75.
26. Mohd. Shkir, V. Ganesh, S. AlFaify, I. S. Yahia & H. Y. Zahran, Tailoring the linear and nonlinear optical properties of NiO thin films through Cr 3+ doping. J. Mater. Sci. Mater. Electron. 29 (2018) 6446–6457.

27. R. BoopathiRaja, M. Parthibavarman, Hetero-structure arrays of $MnCo_2O_4$ nanoflakes@nanowires grown on Ni foam: Design, fabrication and applications in electrochemical energy storage, J. Alloy. Compd. 811 (2019) 152084
28. R. BoopathiRaja, M. Parthibavarman, A. Nishara Begum, Hydrothermal induced novel $CuCo_2O_4$ electrode for high performance supercapacitor applications, Vacuum. 165 (2019) 96-104.
29. R. BoopathiRaja, M. Parthibavarman, Desert rose like heterostructure of $NiCo_2O_4$/NF@PPy composite has high stability and excellent electrochemical performance for asymmetric super capacitor applicationElectrochimica Acta. 346 (2020) 136270
30. R. BoopathiRaja, M. Parthibavarman, Reagent induced formation of $NiCo_2O_4$ with different morphologies with large surface area for high performance asymmetric supercapacitors. Chemical Physics Letters. 755 (2020) 137809
31. R. Ren, H. M. Wei, X. B. Huang, B. Yang,J. N. Ding, Fabrication of NiO nanowires/G composite as electrode material for high performance supercapacitor. Int. J. Electrochem. Sci. 9 (2014) 7206.
32. S. Tougaard, D. Tahir, Electronic and optical properties of Cu, CuO and Cu2O studied by electron spectroscopy, J. Phys.: Condens. Matter. 24 (2012) 175002
33. B. Yao, C. Peng, W. Zhang, Q. Zhang, J. Niu, J. Zhao, A novel Fe(III) porphyrinconjugated TiO_2 visible-light photocatalyst, Appl. Catal., B 174 (2015) 77-84.
34. S. Ghazal, A. Akbari, H.A. Hosseini, Z. Sabouri, F. Forouzanfar, M. Khatami, M. Darroudi, Biosynthesis of Silver-Doped Nickel Oxide Nanoparticles and Evaluation of Their Photocatalytic and Cytotoxicity Properties, Applied Physics A. 126 (2020) 480.
35. S.D. Khairnar, V.S. Shrivastava, Facile Synthesis of Nickel Oxide Nanoparticles for the Degradation of Methylene Blue and Rhodamine B Dye: A Comparative Study. J. Taibah Univ. Sci. 13 (2019) 1108–1118.
36. Z. Ahmad, A.M. Afzal, M.F. Khan, A. Manzoor, H.M.W. Khalil, S. Aftab, Copper-doped nickle-oxide nanoparticles for photocatalytic degradation of erichrome black-T and methylene blue and its solar cell applications, J. Nanoelectron. Optoelectron. 14 (2019) 1304–1312.
37. Deepak Amita, P.S. Arun, Rana, Synthesis, characterization and sunlight catalytic performance of Cu doped NiO nanoparticles, in: AIP Conference Proceedings, AIP Publishing LLC, 2019, 020035.
38. B. Hameeda, A. Mushtaq, M. Saeed, A. Munir, U. Jabeen, A. Waseem, Development of Cu-doped NiO nanoscale material as efficient photocatalyst for visible light dye degradation, Toxin Rev. (2020) 1–11.
39. S. Sankar, S.K. Sharma, N. An, H. Lee, D.Y. Kim, Y.B. Im, Y.D. Cho, R.S. Ganesh, S. Ponnusamy, P. Raji, Photocatalytic properties of Mn-doped NiO spherical nanoparticles synthesized from sol-gel method, Optik 127 (2016) 10727–10734.
40. A. Khatri, P.S. Rana, Visible light photocatalysis of methylene blue using cobalt substituted cubic NiO nanoparticles, Bull. Mater. Sci. 42 (2019) 1–11.

41. M.S.S. Kumar, T.L. Soundarya, G. Nagaraju, G.K. Raghu, N.D. Rekha, F.A. Alharthi, B. Nirmala, Multifunctional Applications of Nickel Oxide (NiO) Nanoparticles Synthesized by Facile Green Combustion Method Using Limonia Acidissima Natural Fruit Juice. Inorg. Chim. Acta 515 (2020) 120059.
42. J.B. Iteku, O. Mbayi, G.N. Bongo, P.K. Mutwale, J.M. Wambale, E. Lengbiye, C.L. Ngunde, K. Ngbolua, Phytochemical Analysis and Assessment of Antibacterial and Antioxidant Activities of Phytolacca Dodecandra L. Herit Leaf Extracts (Phytolaccaceae). Int. J. Biomed. Eng. Clin. Sci. 5 (2019) 31–39.

Figures

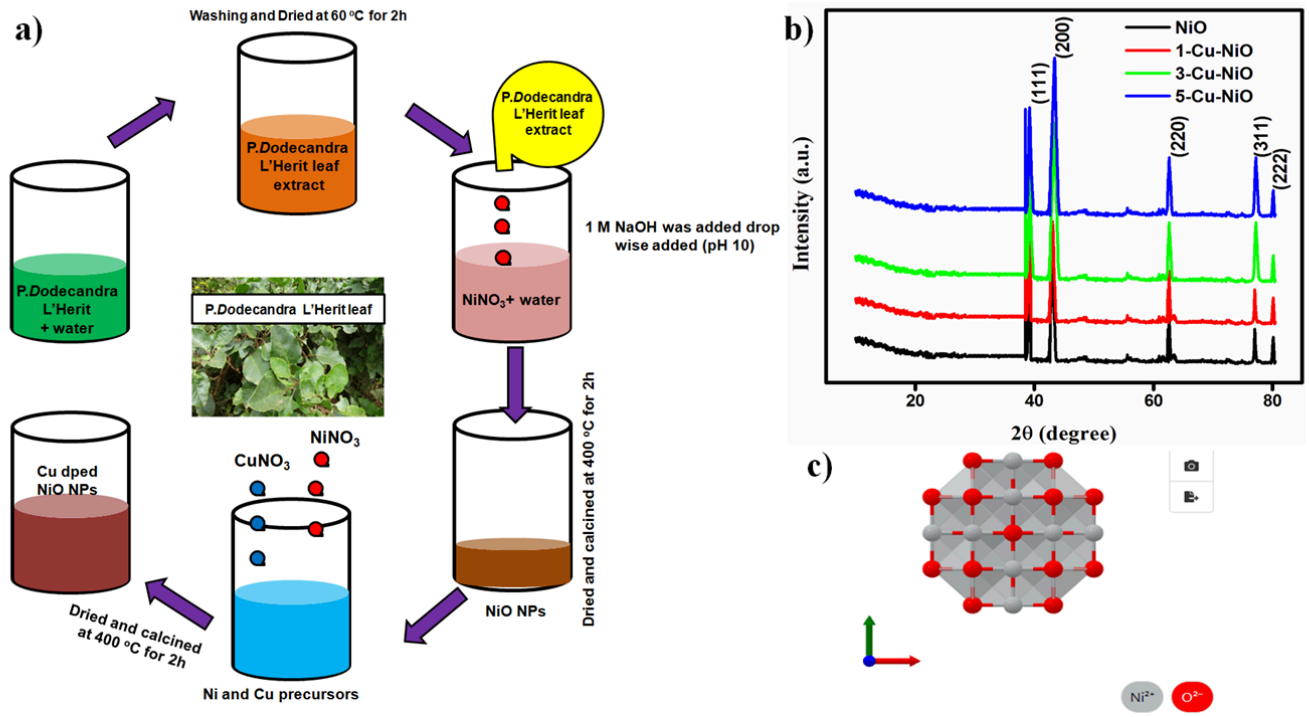

Figure 1

Figure 1

(a) Schematic representation of the synthesis process; **(b)** powder XRD pattern; **(c)** crystal structure of NiO

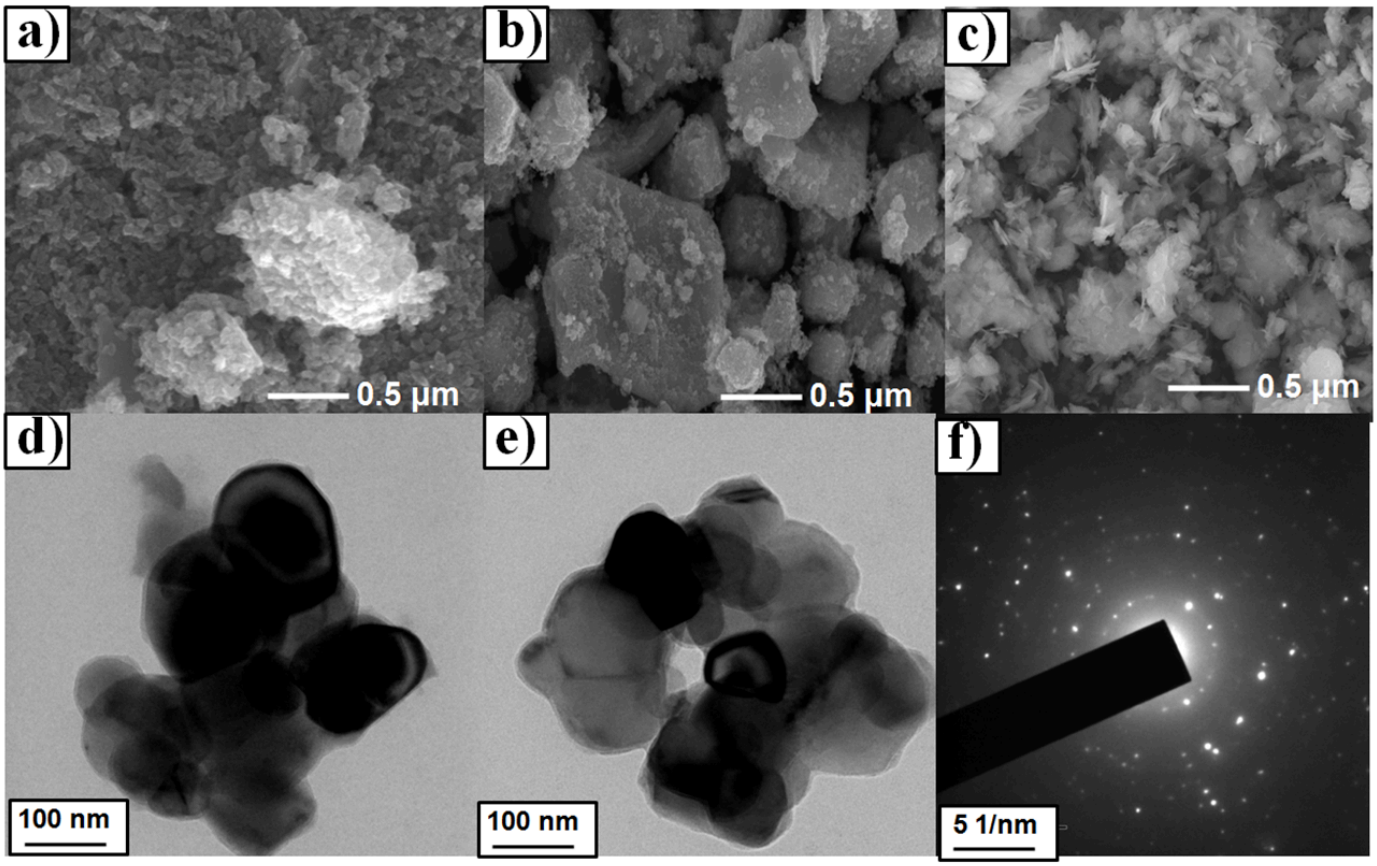

Figure 2

Figure 2

SEM images of **(a)** NiO; **(b)** 1-Cu-NiO; (c) 5-Cu-NiO; TEM image of **(d)** NiO;

(d) 5-Cu-NiO; SAED pattern of 5-Cu-NiO

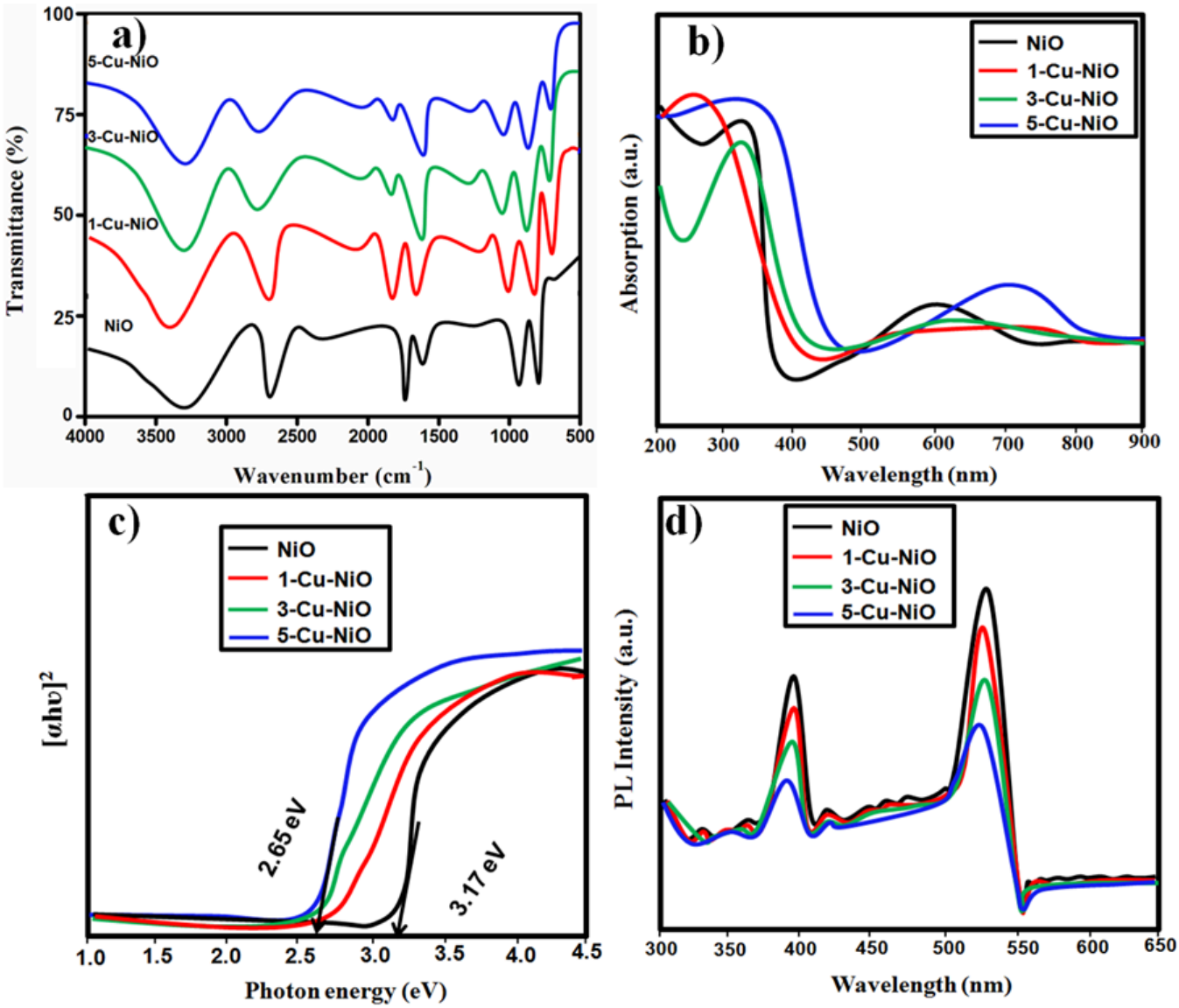

Figure 3

Figure 3

(a) FTIR spectra of photocatalyst samples; **(b)** UV-Vis absorption spectra; **(c)** Band gap plot; **(d)** Room temperature PL spectra of all the photocatalysts with excitation wavelength of 290 nm

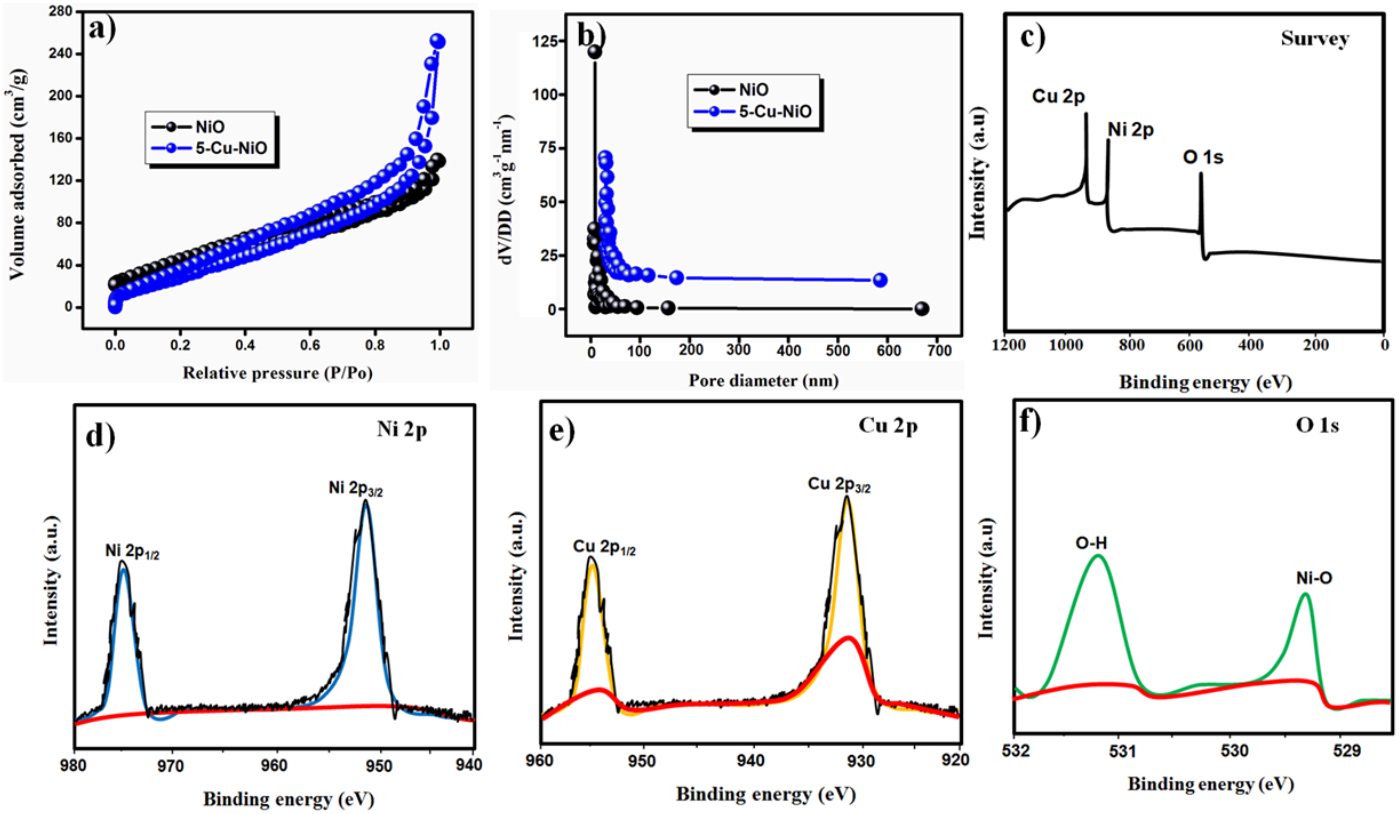

Figure 4

Figure 4

(a) N_2 adsorption desorption isotherm; **(b)** pore size distribution curves of NiO and 5-Cu-NiO; **(c)** XPS survey spectra of 5-Cu-NiO; **(d)** Ni 2p; **(e)** Cu 2p; **(f)** O 1s

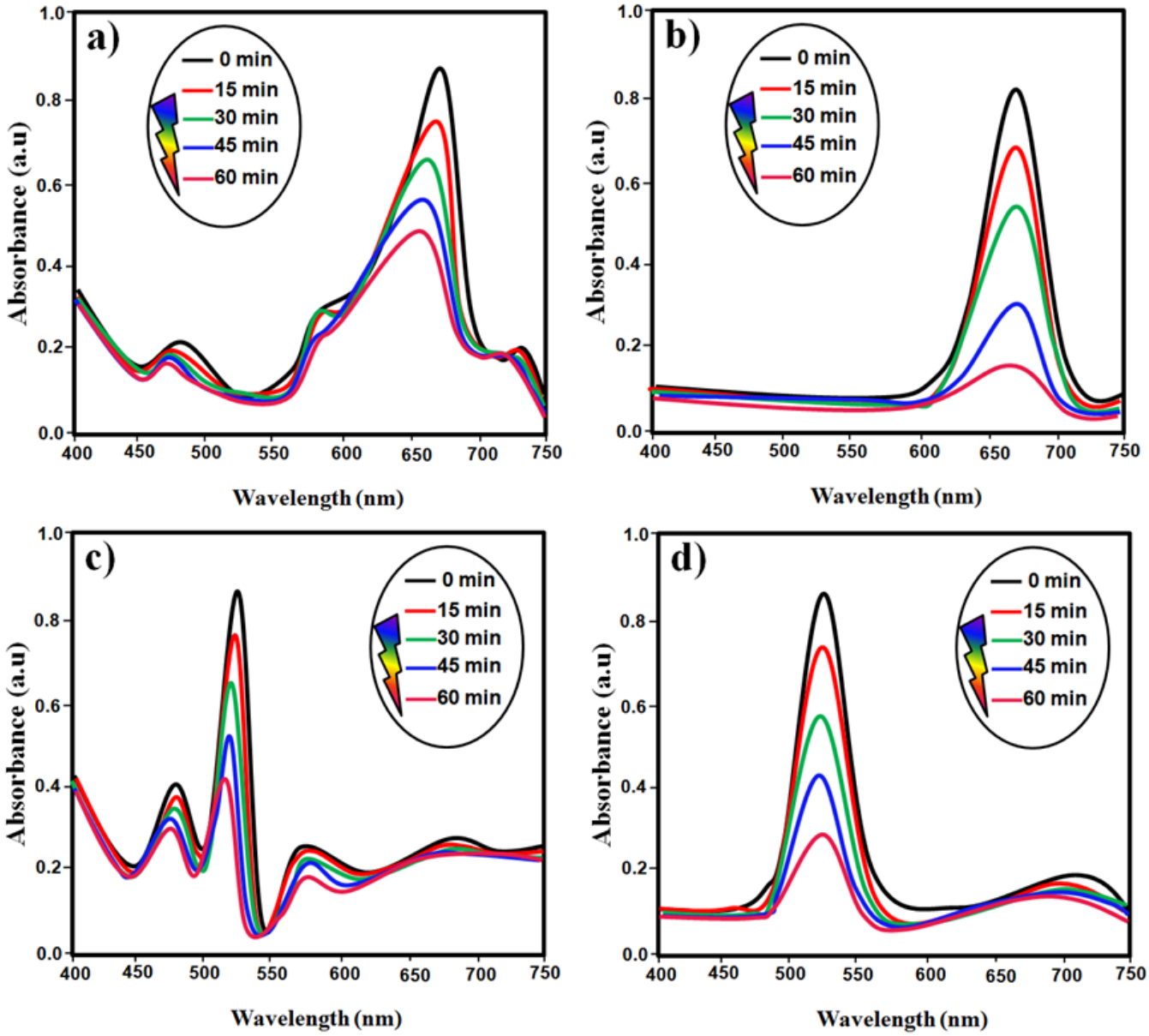

Figure 5

Figure 5

UV absorption spectra of MB over **(a)** NiO and **(b)** 5-Cu-NiO, UV absorption spectra of RB over **(c)** NiO and **(d)** 5-Cu-NiO

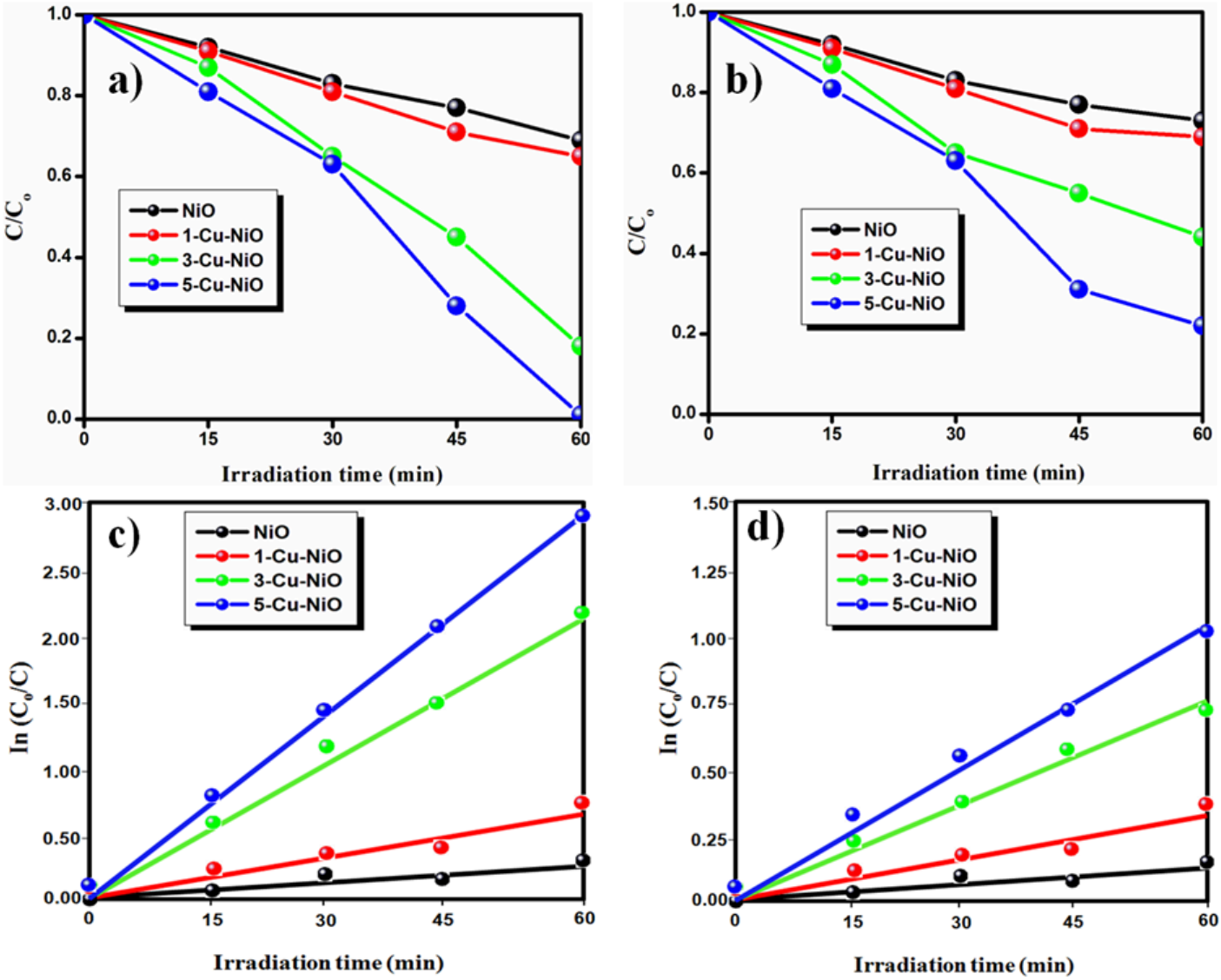

Figure 6

Figure 6

(a)MB degradation efficiency; **(b)** RhB degradation efficiency of all the photocatalyst samples under UV light; first order kinetic plot of **(c)** MB; **(d)** RhB using pure and Cu doped NiO photocatalyst samples

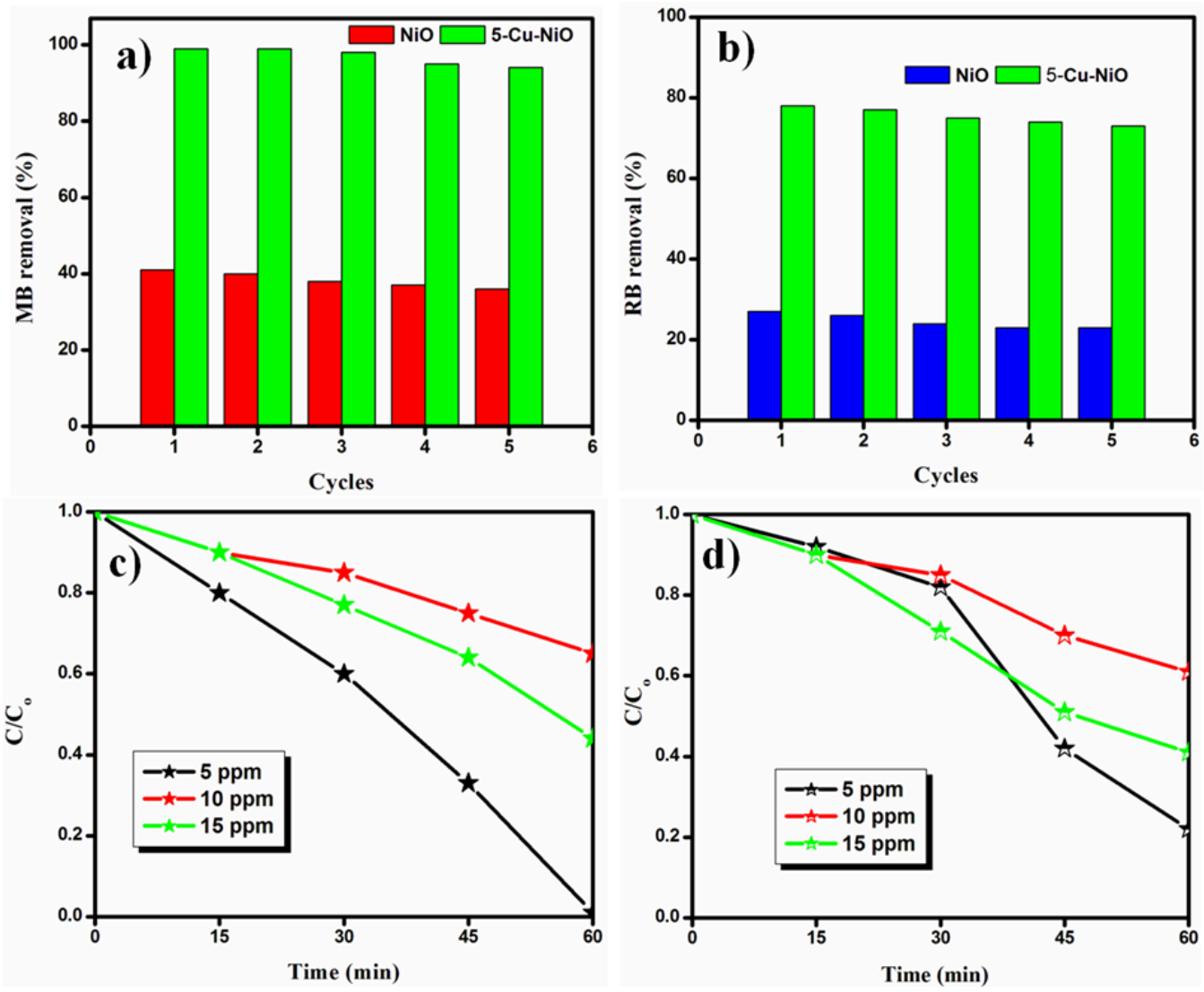

Figure 7

Figure 7

Reusability of the catalyst for (a) MB degradation; (b) RB degradation using pure NiO and 5-Cu-NiO photocatalyst test under UV light exposure; Effects of the initial dye concentration on photocatalytic degradation**(c)** MB; **(d)** RhB

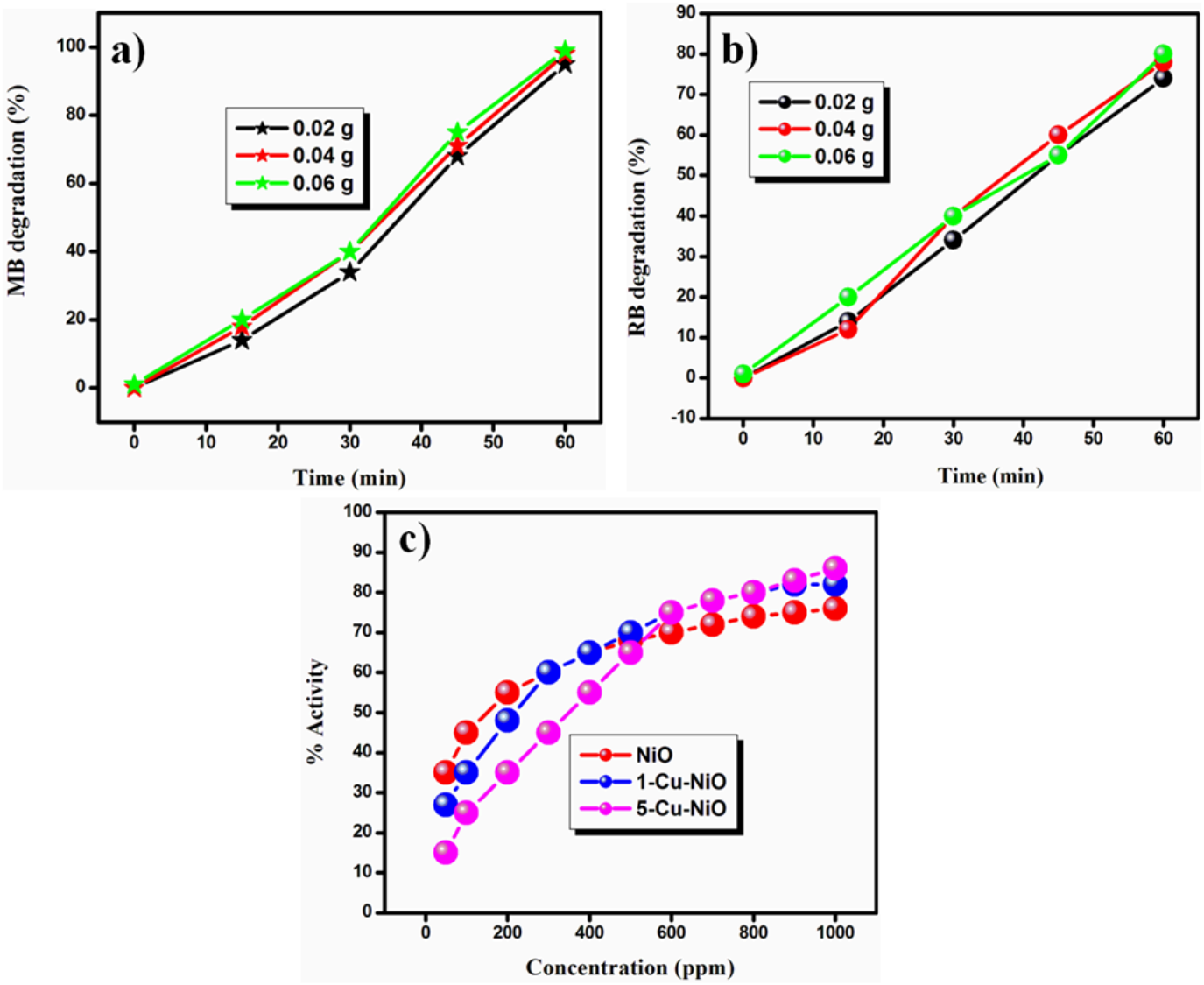

Figure 8

Figure 8

Effect of the irradiation time and catalyst dose on photocatalytic degr (a) MB; (b) RhB under UV light; **(c)** H_2O_2 scavenging activities of NiO and Cu–NiO nanoparticles.

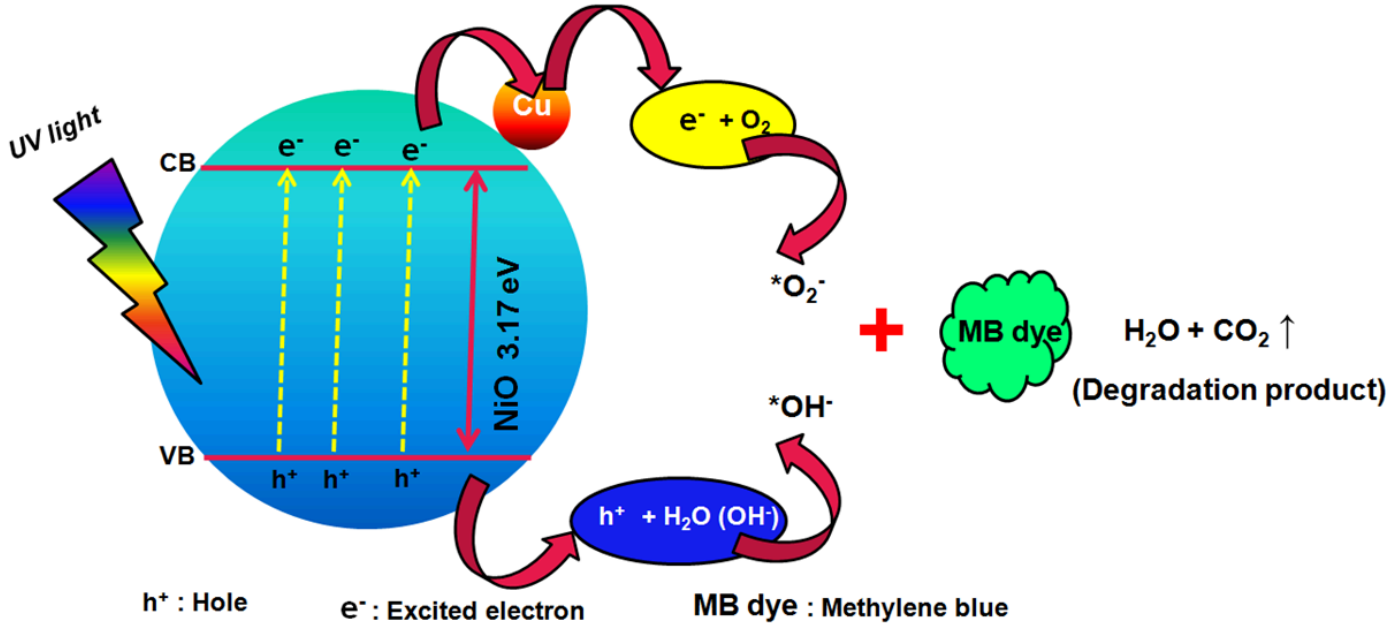

Figure 9

Figure 9

Schematic illustration of mechanism of photocatalytic process of Cu-NiO nanoparticles, under UV irradiation.